Atmos. Chem. Phys., 17, 10037–10050, 2017
https://doi.org/10.5194/acp-17-10037-2017

Atmospheric Chemistry and Physics
Open Access
EGU

Sensitivities of Amazonian clouds to aerosols and updraft speed

Micael A. Cecchini[1,4], Luiz A. T. Machado[1], Meinrat O. Andreae[2,12], Scot T. Martin[3], Rachel I. Albrecht[4], Paulo Artaxo[5], Henrique M. J. Barbosa[5], Stephan Borrmann[2,6], Daniel Fütterer[7], Tina Jurkat[7], Christoph Mahnke[2,6], Andreas Minikin[8], Sergej Molleker[6], Mira L. Pöhlker[2], Ulrich Pöschl[2], Daniel Rosenfeld[9], Christiane Voigt[6,7], Bernadett Weinzierl[7,10], and Manfred Wendisch[11]

[1]Centro de Previsão de Tempo e Estudos Climáticos, Instituto Nacional de Pesquisas Espaciais, Cachoeira Paulista, Brazil
[2]Biogeochemistry, Multiphase Chemistry, and Particle Chemistry Departments, Max Planck Institute for Chemistry, P.O. Box 3060, 55020, Mainz, Germany
[3]School of Engineering and Applied Sciences and Department of Earth and Planetary Sciences, Harvard University, Cambridge, Massachusetts, USA
[4]Departamento de Ciências Atmosféricas, Instituto de Astronomia, Geofísica e Ciências Atmosféricas (IAG), Universidade de São Paulo (USP), Brazil
[5]Instituto de Física (IF), Universidade de São Paulo (USP), São Paulo, Brazil
[6]Institut für Physik der Atmosphäre (IPA), Johannes Gutenberg-Universität, Mainz, Germany
[7]Institut für Physik der Atmosphäre, Deutsches Zentrum für Luft- und Raumfahrt (DLR), Oberpfaffenhofen, 82234 Wessling, Germany
[8]Flugexperimente, Deutsches Zentrum für Luft- und Raumfahrt (DLR), Oberpfaffenhofen, Germany
[9]Institute of Earth Sciences, The Hebrew University of Jerusalem, Jerusalem, Israel
[10]Faculty of Physics, University of Vienna, Boltzmanngasse 5, 1090 Vienna, Austria
[11]Leipziger Institut für Meteorologie (LIM), Universität Leipzig, Stephanstr. 3, 04103 Leipzig, Germany
[12]Scripps Institution of Oceanography, University of California San Diego, La Jolla, CA 92093, USA

Correspondence to: Micael A. Cecchini (micael.cecchini@gmail.com)

Received: 31 January 2017 – Discussion started: 1 March 2017
Revised: 21 June 2017 – Accepted: 13 July 2017 – Published: 28 August 2017

Abstract. The effects of aerosol particles and updraft speed on warm-phase cloud microphysical properties are studied in the Amazon region as part of the ACRIDICON-CHUVA experiment. Here we expand the sensitivity analysis usually found in the literature by concomitantly considering cloud evolution, putting the sensitivity quantifications into perspective in relation to in-cloud processing, and by considering the effects on droplet size distribution (DSD) shape. Our in situ aircraft measurements over the Amazon Basin cover a wide range of particle concentration and thermodynamic conditions, from the pristine regions over coastal and forested areas to the southern Amazon, which is highly polluted from biomass burning. The quantitative results show that particle concentration is the primary driver for the vertical profiles of effective diameter and droplet concentration in the warm phase of Amazonian convective clouds, while updraft speeds have a modulating role in the latter and in total condensed water. The cloud microphysical properties were found to be highly variable with altitude above cloud base, which we used as a proxy for cloud evolution since it is a measure of the time droplets that were subject to cloud processing. We show that DSD shape is crucial in understanding cloud sensitivities. The aerosol effect on DSD shape was found to vary with altitude, which can help models to better constrain the indirect aerosol effect on climate.

1 Introduction

The Amazon Basin can serve as a natural laboratory to study anthropogenic effects on cloud microphysical and radiative properties. In its remote parts, an absence of pollution similar to the preindustrial era still prevails, while in other regions, cities and biomass burning emit high numbers of aerosol par-

ticles into the atmosphere. This is especially important during the dry season, when rainout is less frequent (Artaxo et al., 2002; Kuhn et al., 2010; Martin et al., 2010). Under background conditions, cloud condensation nuclei (CCN) consist mostly of secondary organic aerosol (SOA) particles formed by the oxidation of volatile organic compounds (VOCs), which condense and grow sufficiently to form CCN (Pöschl et al., 2010). Anthropogenic emissions may enhance the oxidation process, leading to increased SOA and CCN concentrations (Kanakidou et al., 2000; Hallquist et al., 2009). Even though aerosol particles can be scavenged by precipitation, nanoparticles produced in the upper troposphere can be transported downwards by deep convective systems, approximately reestablishing the surface aerosol concentration (Wang et al., 2016).

These processes illustrate the complex feedbacks between the vegetation, the aerosols serving as CCN, and the clouds providing water to the vegetation. There are, however, still plenty of open questions. The main difficulty in this regard is the quantitative comparison of the aerosol effect to other processes, given that the anthropogenic influences alter more than just aerosol particle concentrations. Human activities associated with urbanization and agriculture change the local landscape and the Earth's surface properties, also altering the energy budget (Fisch et al., 2004) and consequently the thermodynamic conditions for cloud formation. According to Fisch et al. (2004), the convective boundary layer is deeper over pasture during the dry season because of the increased sensible heat fluxes. This effect results in greater cloud base heights with potentially stronger updrafts, which should also be considered when analyzing the aerosol effect.

One possible way to compare different effects on cloud microphysical properties is through a sensitivity calculation. It can provide specific quantifications of aerosol and thermodynamic effects on cloud microphysical quantities. One such sensitivity study, in which the author calculates cloud droplet number concentration (N_d) sensitivities to several aerosol and thermodynamic drivers, such as total aerosol particle concentration (N_a), updraft speed (w), and liquid water content (LWC), was proposed by Feingold (2003). However, this analysis was limited to adiabatic stratocumulus clouds for which collision–coalescence was not considered. Another modeling study, in which they identified three regimes that modulate the N_d sensitivity, was proposed by Reutter et al. (2009). The regimes are aerosol-limited, updraft-limited, and the transition between them. The authors highlight that the N_d dependence on N_a and w may vary given their relative magnitudes. This study is limited to cloud base, therefore not addressing cloud evolution. The Reutter et al. (2009) study was extended by Chang et al. (2015), who took into account the evolution of the systems by considering the sensitivities on precipitation and ice phase, but was relatively limited in terms of representativeness because of the use of a 2-D model. Satellite studies (e.g., Bréon et al., 2002; Quaas et al., 2004; Bulgin et al., 2008) have an intrinsic limitation given the characteristics of the remote sensors. This kind of study usually deals with vertically integrated quantities and frequently focuses on oceanic regions because of the favorable surface contrast.

The main goal of this study is to expand the sensitivity calculations usually found in the literature to include (1) aerosol and thermodynamic effects on cloud droplet number concentration, size, and shape of the size distribution; (2) comparison with the effect of cloud evolution, i.e., in-cloud processing; and (3) in situ observations of the less frequently studied convective clouds over tropical continental regions. For this purpose, we report on recent measurements over the Amazon rainforest during the ACRIDICON-CHUVA campaign (Wendisch et al., 2016), in which a wide variety (in terms of aerosol concentrations and thermodynamic conditions) of cloud types were probed. We quantify the aerosol-induced changes in cloud microphysical properties and compare them to the effects of updraft intensity, which are related to thermodynamic properties, over different regions in the Amazon. Both processes are analyzed with a focus on cloud evolution. Our methodology should prove useful for better understanding aerosol–cloud interactions over the Amazon, which is a region, as are the tropics as a whole, with poor forecasting skill (Kidd et al., 2013). Section 2 describes the experiment, its data, and the methods used for the analysis. Results are presented in Sect. 3, followed by the conclusions in Sect. 4.

2 Methodology

2.1 Campaign and methodology

During the years 2014 and 2015, the GoAmazon2014/5 campaign took place in the Amazon to improve our understanding regarding aerosol particles, atmospheric chemistry, clouds, radiation, and their interactions (Martin et al., 2016). In conjunction with the second Intensive Operations Period (IOP2) of this experiment, the ACRIDICON-CHUVA campaign took place during September–October 2014 (Wendisch et al., 2016). It included 14 research flights with the German HALO (High Altitude and Long Range Research Aircraft). A previous campaign dedicated to study aerosol–cloud interactions took place in the Amazon in 2002 (LBA-SMOCC; Andreae et al., 2004), but it had been relatively limited in terms of range and ceiling of the aircraft measurements. The high endurance of the HALO aircraft, which carried sophisticated microphysical, aerosol, and solar radiation instrumentation, allowed for long-range flights from remote areas in the northern Amazon to the deforestation arc in the south and to the Atlantic coast in the east (Fig. 1). The flights were planned to cover five different mission types focusing on different cloud, aerosol, chemistry, and radiation processes (see Wendisch et al., 2016, for details). The flights were numbered chronologically as ACXX, in which XX varies from 07 to 20. For this study, the cloud profiling missions are of particular

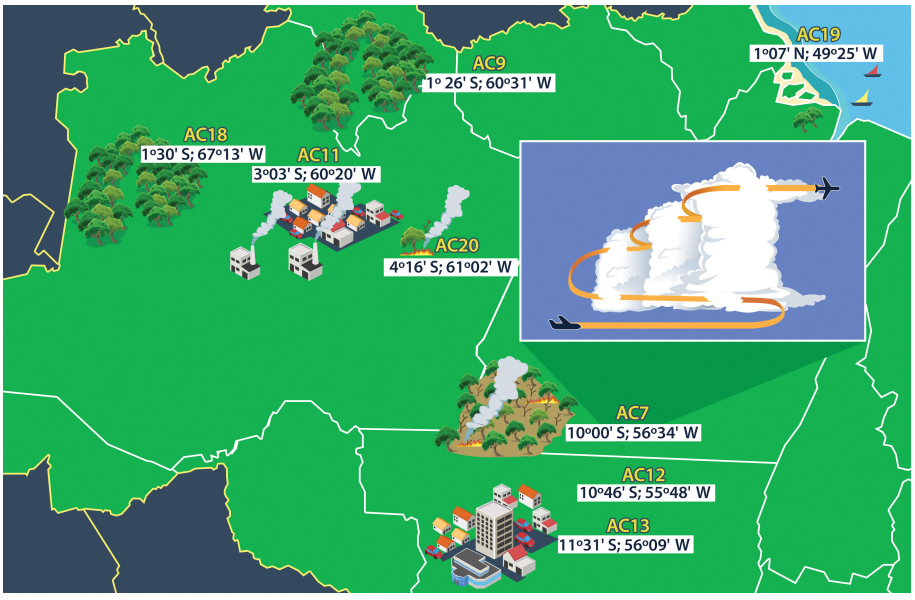

Figure 1. Locations where cloud profiles have been collected for different HALO flights. Clouds formed over southern Amazonia and in the Manaus region are subject to higher aerosol loadings due to the presence of the deforestation arc and urban emissions. Clouds formed over the northern and northwestern Amazon are driven by background conditions with low aerosol concentration. During the GoAmazon2014/5 IOP2, maritime clouds were also profiled on the Atlantic coast.

interest and their respective locations are shown in Fig. 1. In this study, we take advantage of HALO's capabilities of comparing different types of clouds formed over different Amazonian regions, focusing on their warm microphysics. In addition to the HALO measurements, ground-based equipment was also operated in and near Manaus city (Machado et al., 2014; Martin et al., 2016).

The results shown here were obtained from the measurements of four different instruments (for a list of all HALO instruments, see Wendisch et al., 2016), covering aerosol, cloud, and meteorological properties. We will focus on aerosol and CCN number concentrations, cloud droplet size distributions (DSDs), and updraft speed. The instruments are briefly described below.

2.1.1 CCP

For the cloud droplet size distribution measurements, a modified cloud combination probe (CCP, manufactured by Droplet Measurement Technologies, Inc., Boulder, CO, USA) was adopted on HALO covering an overall size diameter range from 3 to 950 µm. The probe consists of two separate instruments, the CDP (cloud droplet probe; Lance et al., 2010; Molleker et al., 2014) and a grayscale optical array imaging probe (CIPgs, cloud imaging probe; Korolev, 2007). By means of a two-dimensional shadow cast technique, the CIPgs detects cloud particles with size diameters ranging from 15 to 2000 µm. The in-house-developed analysis algorithm from the Max Planck Institute for Chemistry and the Institute for Atmospheric Physics in Mainz sizes and sorts the recorded images into bins of roughly 15 µm width depending on particle shapes and dimensions. The CDP is an optical particle counter (OPC) that detects scattered laser light (in forward direction) arising from individual particles passing through the illuminated optical sample area (Lance et al., 2010; Molleker et al., 2014). The optical sample area has a cross section of 0.2 mm^2 (±15 %) perpendicular to the flight direction. The CDP detects particles with sizes from 3 to 50 µm and classifies these into size histograms of bin widths between 1 and 2 µm. In addition to size histograms recorded at 1 Hz frequency, the CDP stores single-particle data (signal amplitude and microsecond-resolved detection time) of continuous intervals with up to 256 particles every second. This feature can be used to assess the spatial distribution of the droplets in case of multimodal size distributions (Klingebiel et al., 2015). The main uncertainties for the CCP size distributions are due to the uncertainty of the sample area (and thus the scanned air volume), as well as counting statistics. We applied a filter to eliminate DSDs with concentrations lower than 1 cm^{-3} for $D<50$ µm or lower than 0.1 cm^{-3} for $D>50$ µm.

2.1.2 AMETYST-CPC

The aerosol concentrations used in this study refer to the total concentration of particles measured with a butanol-based condensation particle counter (CPC). Four CPCs were deployed on HALO as part of the new basic aerosol instrument package for HALO named AMETYST (Aerosol MeasuremenT sYSTem) and which also includes two Grimm 1.129

Table 1. Definition of the symbols and abbreviations discussed in this study.

Symbol/abbreviation	Definition
DSD	Droplet size distribution
N_d	Cloud droplet number concentration (cm^{-3})
D_{eff}	Effective diameter (μm)
LWC	Liquid water content (gm^{-3})
ε	Relative dispersion parameter (dimensionless)
Λ	Gamma DSD curvature parameter (μm^{-1})
μ	Gamma DSD shape parameter (dimensionless)
N_0	Gamma DSD intercept parameter ($cm^{-3}\,\mu m^{-1-\mu}$)
M_p	DSD moment of order p
D_a	Mean diameter obtained as M_2/M_1 (μm)
γ	Parameter associated with DSD shape, given by $\frac{\Lambda\varepsilon^2}{D_a}$ (μm^{-2})
N_a	Aerosol number concentration (cm^{-3})
w	Updraft speed (ms^{-1})
H	Altitude above cloud base (m)
CCN	Cloud condensation nuclei number concentration (cm^{-3})

OPCs, a two-channel thermal denuder operated at 250 °C, a Radiance Research three-wavelength PSAP (particle soot absorption photometer), and optionally two DMAs (differential mobility analyzers). AMETYST is operated behind the HALO sub-micrometer aerosol inlet (HASI). The CPCs are Grimm 5.410 models, operating at two different flow rates. The CPC internal butanol saturation setting is user-selectable to vary minimum detectable particle sizes. Data used in this study were obtained from $0.6\,L\,min^{-1}$ 5.410 CPC set to a nominal lower cutoff size of 10 nm. Concentrations reported are normalized to standard temperature and pressure conditions. Original data are recorded at 1 Hz temporal resolution. In-cloud data at altitudes below 9 km were removed from the dataset based on cloud probe data (here CAS-DPOL instrument of DLR) to exclude apparent sampling artifacts of the inlet in the presence of liquid droplets in clouds.

2.1.3 CCNC

A cloud condensation nuclei counter (CCNC) was used to obtain CCN number concentrations. The instrument has two columns with a continuous-flow longitudinal thermal gradient in which the aerosol particles are subject to controlled supersaturation (S) conditions. When particles travel longitudinally in the center of each column, they grow by water condensation (depending on their physical and chemical compositions) and are counted as CCN if they reach 1 μm in size (1 Hz sampling rate). The CCNC is manufactured by Droplet Measurement Technologies (DMT) – Roberts and Nenes (2005). Calibrations were performed between flights following Rose et al. (2008). At one column, S was set to be relatively constant at $S \approx 0.55$ %, while the other was subject to 100 s stepping variations between 0.2 and 0.55 %.

2.1.4 BAHAMAS

Vertical wind speeds were obtained from the Basic Halo Measurement and Sensor System (BAHAMAS) sensor installed at the nose of the aircraft (Wendisch et al., 2016). The 3-D wind measurements were calibrated following Mallaun et al. (2015), resulting in an uncertainty of $0.3\,m\,s^{-1}$ for the horizontal components and $0.2\,m\,s^{-1}$ for the vertical components.

2.2 Sensitivity calculation

Several earlier studies calculated cloud sensitivity to aerosols and/or updrafts (Feingold, 2003; McFiggans et al., 2006; Kay and Wood, 2008; Reutter et al., 2009; Sorooshian et al., 2009; Kardys et al., 2012; Chang et al., 2015), but they were usually limited in scope by not individually considering the factors that contribute to the cloud microphysics. This study aims to expand the sensitivity methodology by concurrently considering cloud evolution, updraft speed, and aerosol effects on clouds and by taking advantage of the comprehensive ACRIDICON-CHUVA dataset to represent different kinds of clouds and thermodynamic conditions. As pointed out by Seinfeld et al. (2016), major field campaigns provide a key opportunity for improving our knowledge of the aerosol–cloud–climate interactions, further motivating the results to be presented here.

Three factors will be considered as the main drivers of cloud microphysical properties, each representative at least partially of thermodynamic and aerosol conditions and cloud evolution. Those factors, and other parameters discussed in this study, are defined in Table 1. For the aerosol characterization, we will use averaged concentrations measured by the AMETYST CPC (referred here as N_a – see Tables 1 and 2) at the cloud base level. This level was obtained from the CCP–

Table 2. N_a and CCN at cloud base for each flight considered in this study. *CCN concentrations for flight AC20 showed pronounced scaling with S. The value shown is for the measurements in which $S>0.52\,\%$. This value is closer to the maximum droplet concentration measured at the base of the clouds ($=1422\,cm^{-3}$).

Flight	N_a (cm^{-3})	CCN (cm^{-3})	S (%)
AC19	465	119	0.52
AC18	744	408	0.50
AC9	821	372	0.51
AC20	2331	1155*	0.55
AC7	2498	1579	0.50
AC11	2691	1297	0.49
AC12	3057	2017	0.44
AC13	4093	2263	0.44

CDP measurements as the lowest level at which the LWC is higher than $0.01\,g\,m^{-1}$. As the profiles always started with cloud base penetrations, this ensures a precise estimation of cloud base altitude. Table 2 also shows that CCN concentrations were proportional to N_a for the chosen instrument supersaturation. A linear fit between N_a (as the dependent variable) and CCN (as the independent variable) results in $R^2 = 0.96$, with angular and linear coefficients equal to 1.57 and $243\,cm^{-3}$, respectively. For the purposes of the sensitivity calculations, we will use N_a instead of CCN concentrations because they are not dependent on instrument or cloud supersaturations. It is known that polluted clouds tend to have lower supersaturations given the enhanced condensation. Therefore, the use of constant-supersaturation CCN concentrations does not provide a common benchmark between the clouds probed here. Conversely, it is difficult to obtain the supersaturation within the clouds and the consequent CCN concentration modulation. In that regard, N_a proved to be most adequate for providing a framework to compare polluted and clean clouds. The sensitivity calculation (see below) uses derivatives of the concentrations; thus, the choice of N_a or CCN should have no significant impact on the results to be presented here (because of the linear correlation between CCN and N_a). The most pristine clouds are observed near the coast (AC19), followed by the ones measured over the forest. The flights AC7, AC12, and AC13 each showed increasing aerosol concentrations as the flights moved towards the southern Amazon. For the flights closer to Manaus city, the aerosol loading of the clouds depends on localized aspects such as small-scale biomass burning and the pollution plume from urban and/or industrial activities (Cecchini et al., 2016). In this study, we will focus on aerosol number concentrations, and their chemical composition will not be addressed.

The second factor that affects cloud microphysics is the updraft intensity (w). It, along with the aerosol population, defines the supersaturation inside the clouds and thus affects the droplets' condensational growth. The intensity of the updrafts depends both on meteorological conditions (e.g., temperature and humidity profiles) and on the latent heat release of condensing water. Aerosols may indirectly affect the amount of latent heat released (smaller droplets in polluted clouds have a favorable area-to-volume ratio), but the speed of the ascending air can be understood as a response to the thermodynamic conditions in the clouds. Therefore, w can be used as a benchmark to compare different clouds subject to similar thermodynamic conditions relevant to cloud microphysics.

Lastly, it is important to have an estimate of how cloud microphysical properties evolve throughout the system evolution, but more importantly, how to detect similar cloud stages over the different flights for comparison. The HALO cloud profiling missions were planned to capture growing convective clouds in the different Amazonian regions. The aircraft penetrated the systems first at cloud base and then at ascending altitudes in the cloud tops of the growing convective elements. This strategy allows the use of altitude above cloud base (herein referred as H, in meters, also known as cloud depth) as a proxy for cloud evolution. Measurements at higher altitudes reflect later stages of the cloud life cycle as the systems develop upward. We use the derivatives of the microphysical properties with respect to H, which can be understood as variations during the cloud evolution. This will put the sensitivities to N_a and w into perspective, highlighting the importance of detecting cloud stage. It could be argued that the ratio H/w would be a more direct estimate of the cloud lifetime, given that it is the time that it took for the cloud to reach H. However, this approach would need prescribed w profiles below each measurement, which is not feasible in this study given that different clouds can be measured in the same profiling mission. Additionally, there is high w variability horizontally between the cloud edges and cores, adding extra complexity. Therefore, we will use H as the proxy for cloud evolution even though it does not represent cloud lifetime directly (i.e., does not have units of time). The profiling strategy of measuring growing convective clouds favors this interpretation.

The sensitivities are calculated as partial derivatives on a natural log scale. In this way, they are normalized for quantitative comparison. Based on the terminology in the literature (e.g., Feingold, 2003; Chang et al., 2015), we consider the sensitivities as follows:

$$S_Y(X_i) = \left.\frac{\partial \ln Y}{\partial \ln X_i}\right|_{X_j, X_k}, \quad (1)$$

in which X is the independent variable, i.e., w, N_a, and H, and Y is the cloud microphysical property of interest. For the sensitivity calculation, we will focus firstly (Sect. 3.2) on cloud droplet number concentration (N_d) and effective droplet diameter (D_{eff}) of cloud DSD with $D<50\,\mu m$. In Sect. 3.3 we also consider the sensitivities in LWC, relative dispersion (ε), and curvature parameter (Λ; see respective text for details). The three factors chosen for X in this study

are not necessarily independent; therefore, in order to follow the partial derivative formalism, we include the criteria expressed by the vertical line (Eq. 1). The subscript in X identifies the different independent variables considered. This notation means that two independent variables remain constant while the sensitivity to the third is being calculated. As an example, the sensitivity of N_d to N_a, w, and H can be expressed as

$$S_{N_\mathrm{d}}(N_\mathrm{a}) = \left.\frac{\partial \ln N_\mathrm{d}}{\partial \ln N_\mathrm{a}}\right|_{w,H}, \qquad S_{N_\mathrm{d}}(w) = \left.\frac{\partial \ln N_\mathrm{d}}{\partial \ln w}\right|_{N_\mathrm{a},H},$$
$$S_{N_\mathrm{d}}(H) = \left.\frac{\partial \ln N_\mathrm{d}}{\partial \ln H}\right|_{w,N_\mathrm{a}}. \tag{2}$$

Equation (2) recognizes that several parameters can affect N_d, and they should be analyzed individually. Other sensitivities, such as $S_{D_\mathrm{eff}}(N_\mathrm{a})$ or $S_{D_\mathrm{eff}}(w)$, are obtained analogously.

As it is not feasible to analyze the sensitivities under exactly constant conditions as in Eq. (2), we decided to use N_a, w, and H intervals instead. These quantities were binned into $\{0, 500, 1000, 3000, 4500\,\mathrm{cm}^{-3}\}$, $\{0, 0.5, 1, 2, 4, 8\,\mathrm{m\,s}^{-1}\}$, and $\{0, 200, 500, 950, 1625, 2637, 4156\,\mathrm{m}\}$, respectively. In this way, there are 4, 5, and 6 N_a, w, and H intervals, respectively. The values of the bins were chosen in order to maximize the number of data in each interval, which required growing spacing in w and H. We use constant N_a values for each profile and the respective bins effectively group different flights according to the pollution level. Note that flight AC19 falls in the first interval; flights AC9 and AC18 in the second; AC7, AC11, and AC20 in the third; and AC12 and AC13 in the fourth (see Table 2). We then produce 4-by-5-by-6 matrices containing averaged N_d and D_eff values for the combined intervals, covering all variations possible. The sensitivities are calculated as follows: 1) firstly, we choose one independent variable for the sensitivity calculation, which corresponds to one dimension of the matrix; 2) the other two dimensions are then fixed and we obtain the individual curve representing the relation between N_d or D_eff and the independent variable of choice; 3) the sensitivity is calculated as the linear fit of this curve on the natural logarithm scale (in order to be normalized); 4) the process is repeated for every combination of dependent and independent variables possible. Different bin configurations were tested and the results proved to be relatively insensitive to the bin number and width.

3 Results

3.1 Cloud droplet size distributions related to different aerosol and thermodynamic conditions

The first qualitative indication of the effect of N_a, w, and H on cloud microphysical properties can be seen in Fig. 2. This figure shows DSDs ($\mathrm{d}N/\mathrm{dlog}D$ in the vertical axis) grouped into four categories according to the aerosol concentration (N_a) at cloud base: (1) maritime clouds, with $N_\mathrm{a} \leq 500\,\mathrm{cm}^{-3}$; (2) clouds under Amazonian background conditions, with $500\,\mathrm{cm}^{-3} < N_\mathrm{a} \leq 1000\,\mathrm{cm}^{-3}$; (3) moderately polluted clouds, with $1000\,\mathrm{cm}^{-3} < N_\mathrm{a} \leq 3000\,\mathrm{cm}^{-3}$; and (4) polluted clouds, with $N_\mathrm{a} > 3000\,\mathrm{cm}^{-3}$. Solid lines in Fig. 2 represent DSDs for neutral vertical speed ($-1\,\mathrm{m\,s}^{-1} \leq W \leq 1\,\mathrm{m\,s}^{-1}$), while the DSDs with dashed and dotted–dashed lines indicate the updraft and downdraft regions, respectively ($|W| > 1\,\mathrm{m\,s}^{-1}$; note that we use W to differentiate from w, which refers only to the updraft portion). They represent averages for all profiles matching the aerosol intervals chosen (one maritime, two Amazonian background conditions, three moderately polluted, and two polluted). Individual profiles can be found in the Supplement (Figs. S1–S4). In general, all profiles show droplet growth with altitude as they continually go through the condensational and collision–coalescence processes. The enhanced DSD widening with altitude presented in Fig. 2a, b suggests relative predominance of collision–coalescence. Those observations also support the choice of H as a proxy for cloud lifetime.

From Fig. 2, it is evident that aerosols and updrafts affect the droplet size distribution and its evolution in different ways and magnitudes. Clouds that develop under similar aerosol conditions tend to have similar DSDs not only at cloud base but also higher in the warm layer. The individual profiles shown in Figs. S1–S4 confirm the pattern that is evident in Fig. 2. Conversely, the updraft effect is limited to modulations of the DSDs, especially in the $D < 10\,\mu\mathrm{m}$ range. Note that DSDs subject to similar w values can be widely different depending on the respective pollution. The resulting vertical evolution of the clouds is dependent on the N_a value, being more pronounced the cleaner the clouds are. We only observed significant concentrations of precipitation-sized droplets (e.g., $> 100\,\mu\mathrm{m}$) for $N_\mathrm{a} < 3000\,\mathrm{cm}^{-3}$.

The main motivation for calculating sensitivities is to quantify and compare the role of N_a, w, and H in the formation and evolution of the DSDs as seen in Fig. 2. In this way, it will be possible to check the magnitudes of the effects of aerosols, thermodynamics (as seen from the updrafts), and cloud evolution in the determination of the warm-phase characteristics. Note, however, that we are focusing on only one portion of the updraft effects, i.e., the condensation and collision–coalescence effects. For instance, Heymsfield et al. (2009) showed that small droplets carried up by updrafts can significantly participate in the cold processes of the clouds, which are not addressed here. This study considers the first stage of the cumulus clouds just before the formation of ice particles. Regardless, Fig. 2 shows evidence that all three chosen independent variables have specific roles in determining cloud DSD characteristics. Together they explain most of the warm-phase properties.

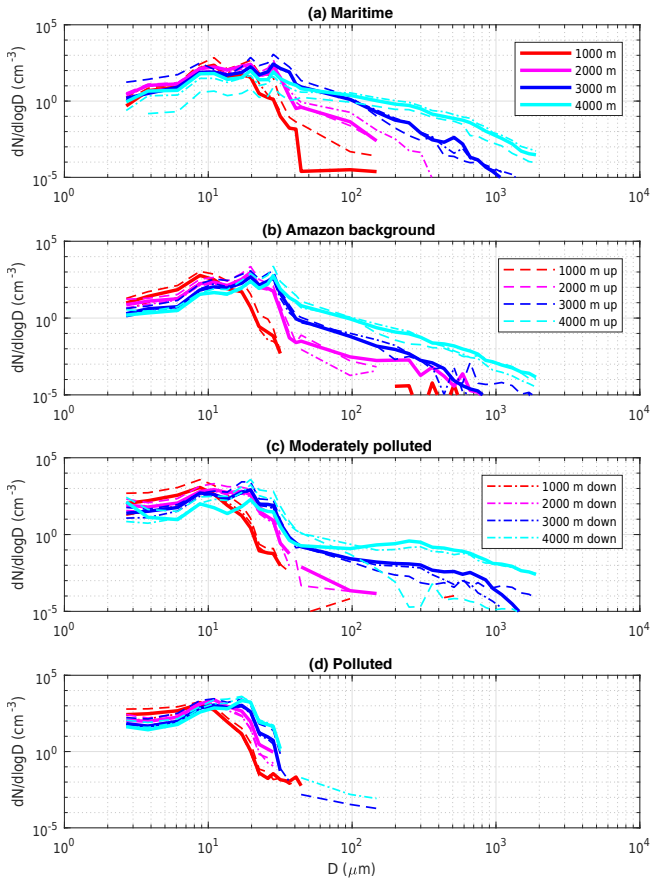

Figure 2. Droplet size distributions as functions of altitude above cloud base, aerosol particle number concentration, and vertical wind speed (W). Four 1000 m thick layers are considered in the vertical, and the legends in the graphs show the respective upper limit of each one. Solid lines represent averaged DSDs for $-1\,\mathrm{m\,s^{-1}} \leq W \leq 1\,\mathrm{m\,s^{-1}}$, i.e., for relatively neutral vertical movements. Dashed lines represent averaged DSDs for the updraft regions where $W > 1\,\mathrm{m\,s^{-1}}$, and dotted–dashed lines represent the downdrafts ($W < -1\,\mathrm{m\,s^{-1}}$).

3.2 Comparing the main drivers of bulk microphysical properties of Amazonian clouds

For quantitative comparisons, it is interesting to consider bulk DSD properties such as N_d and D_eff instead of the whole DSD as in Fig. 2. We will quantify the influence of N_a, w, and H in these properties as a means of understanding the effects on the overall DSD. This analysis will be complemented by the study of the DSD shape in the next section. By comparing the sensitivities of cloud droplet concentration and size to N_a and w, it is possible to make a comparison that represents, at least partially, the contrasts between the importance of aerosols and thermodynamics in cloud characteristics. A significant portion of the previous work in this field was dedicated to understanding the processes that lead to the observed N_d. Twomey (1959) provides theoretical considerations of N_a and w effects on the supersaturation, which ultimately defines N_d for a given CCN spectra. More recent studies report on observations and modeling efforts to portray these processes in different regions of the world, calculating cloud sensitivities to both updraft speed and aerosol conditions. By analyzing aerosol and updraft conditions around the globe, Sullivan et al. (2016) note that w can be the primary driver of N_d in some regions. Reutter et al. (2009), using an adiabatic cloud model, argue that N_d sensitivities to aerosol concentrations and w can vary depending on their relative magnitudes. Adiabatic clouds are not highly sensitive to w (at cloud base) when CCN concentrations are low and vice versa. Some studies also consider sensitivities in droplet size, such as Feingold (2003). However, cloud evolution is rarely put into perspective representing a limitation of previous studies. In the following, we will show our extended calculations of the sensitivities, in which we consider the effects of aerosols, updraft speed, and H on N_d and D_eff.

Based on Eq. (2), it is evident that there exist several values for each sensitivity. As an example, $S_{N_\mathrm{d}}(N_\mathrm{a})$ has different values depending on the chosen pair of $\{w, H\}$. However, given the nature of in situ measurements, individual $S_{N_\mathrm{d}}(N_\mathrm{a})$ values are associated with reduced sample sizes and, therefore, compromise the statistical confidence. In this case, we present averaged values and the respective standard deviation for all $\{w, H\}$ pairs considered, applying the same calculation to the other sensitivities as well. The intervals chosen for N_a, w, and H imply that those averages are representative of the lower ~ 4 km of the clouds, with updrafts up to $8\,\mathrm{m\,s^{-1}}$ and aerosol concentrations ranging from 500 to $4500\,\mathrm{cm^{-3}}$.

The results of the N_d and D_eff averaged sensitivities (Table 3) reflect the patterns observed in Fig. 2. The effective diameter shows strong association with the aerosol concentration and H while being almost independent of w. Specifically regarding N_a, the sensitivities calculated represent the first step in the parameterization of the aerosol indirect effect for climate models, i.e., its relation to cloud microphysical properties. Multiple studies have focused on this issue from several observational setups such as satellite or surface remote sensing and in situ measurements. Pandithurai et al. (2012) provide a compilation of this type of calculation (see their Table 2), showing a high variability among the sources. According to Schmidt et al. (2015), the differences are due to not only the measurement setup but also to the region (ocean or land), the types of clouds, and the differences in the methodologies. Remote sensing techniques often retrieve vertically integrated quantities at relatively rough horizontal resolution, which can smooth the results, meaning lower sensitivities. Conversely, in situ airborne measurements are closer to the process scale and may result in more accurate estimates of the aerosol effect (Werner et al., 2014). However, the studies reviewed in Pandithurai et al. (2012) and Schmidt et al. (2015) are mostly for stratus or cumulus clouds over ocean. Additionally, measurements of w were either not available or were not differentiated in most of the

previous analyses, while the results are often integrated in altitude or limited to a specific cloud layer (e.g., cloud top in satellite retrievals). Our study focuses on tropical convection over the Amazon and takes into account both the updraft speed and altitude of the measurements.

The values of the sensitivities with regard to N_a presented here are among the highest reported in literature. They are not far from the theoretical limit of $S_{N_d}(N_a) = 1$ ($N_d \leq N_a$) and $S_{D_{eff}}(N_a) = -0.33$, which is quite common for in situ airborne studies (Werner et al., 2014). The limit for D_{eff} is an approximation and stems from the relation (if LWC is held constant) $D_{eff} \propto \left(\frac{LWC}{N_d}\right)^{1/3}$ (e.g., Martin et al., 1994). Given the precautions taken here to isolate the aerosol effects, these values show that Amazonian clouds are highly sensitive to pollution. Human-emitted particles affect not only the DSDs close to cloud base but also over at least the lower 4 km of the warm-phase domain. The meteorological and cloud morphology conditions in the Amazon also seem to enable the high sensitivity values found. A previous study by Vogelmann et al. (2012) found relatively invariant N_d as a function of N_a. Beyond instrumental and methodological differences, this study also focused on shallow (200 to 500 m thickness) broken clouds with weak updrafts over Oklahoma. This type of cloud favors the entrainment mixing feedback, in which polluted clouds tend to have lower LWC because of enhanced droplet evaporation. The differences between the results shown here and the study of Vogelmann et al. (2012) suggest that the entrainment mixing process is not dominant over the Amazon. Possible reasons include abundant water vapor, thicker clouds, stronger convection and updrafts, and low vertical wind shear. High humidity of the surrounding air induces weaker LWC and N_d depletion by the entrainment mixing process (see, for instance, Korolev et al., 2016) because of slower evaporation. Stronger convection induces deeper clouds that have a relatively low area-to-volume ratio as compared to the clouds reported in Vogelmann et al. (2012). Therefore, the entrainment at cloud edges are not as dominant. Low area-to-volume ratios are also favored by the weak vertical wind shear typical of tropical regions. This mechanism was studied in Fan et al. (2009), who concluded that convection invigoration is favored under low vertical wind shear conditions, while the opposite happens with high vertical wind shear.

The sensitivities to the updraft speed have a distinct behavior when compared to the aerosol effect. Not only does it show lower values overall but it also shows different behaviors for N_d and D_{eff}. It shows that even strong updrafts are not able to significantly increase the effective droplet size by enhancing condensation. In fact, this sensitivity oscillates around zero with slightly negative and positive values (see Table S2) and with relatively low R^2 values. This finding is similar to what Berg et al. (2011) observed in Oklahoma City. Close to cloud base, they found a significant relation between N_d and w and a low correlation between D_{eff} and w. Here we show that this feature is not limited to cloud base but persists with altitude on average. Feingold (2003), using an adiabatic cloud parcel model, found a negative value for $S_{D_{eff}}(w)$, with a higher absolute value for polluted clouds. The result could be explained by activation of smaller aerosol particles with increasing updraft speed, leading to higher concentrations of small droplets that skewed the mean diameter to lower values. Although we observed slightly negative sensitivity for highly polluted clouds at their base (Table S2), our measurements show that the overall averaged D_{eff} is nearly independent of w for the Amazonian clouds.

Table 3. N_d and D_{eff} averaged sensitivities to N_a, w, and H. Standard deviations are also shown. R^2 values are averages of the individual fits. The total variations for N_a, w, and H are 500 to 4500 cm^{-3}, 0 to 8 $m\,s^{-1}$, and 0 to 4156 m, respectively. Intervals grow logarithmically (or close to) for w and H.

	$\overline{S_{N_d}}$	$\overline{S_{D_{eff}}}$
N_a	0.84 ± 0.21 $R^2 = 0.91$	-0.25 ± 0.074 $R^2 = 0.89$
w	0.43 ± 0.28 $R^2 = 0.81$	0.028 ± 0.058 $R^2 = 0.46$
H	-0.13 ± 0.16 $R^2 = 0.38$	0.28 ± 0.058 $R^2 = 0.93$

Freud et al. (2011) and Freud and Rosenfeld (2012) showed similar observations in the Amazon, India, California, and Israel. They provide theoretical formulations that support some of those observations. These authors showed that the vertical evolution of D_{eff} behaves almost adiabatically because of the predominance of inhomogeneous mixing in convective clouds. In this way, droplet effective size can be obtained from cloud base N_d, pressure, and temperature. In fact, this is the framework for a new technique developed to obtain CCN retrievals from satellites (Rosenfeld et al., 2016). Our study provides a new look at those observations and theoretical considerations by specifically quantifying, without any adiabatic assumption, each process with our formulation of sensitivity.

Comparisons of the sensitivities to w and N_a can be used to infer the roles of the aerosols and thermodynamic conditions in the DSD characteristics. Not only do the aerosols primarily determine the size of the droplets but they also have the biggest impact on the number concentration, high variability in $S_{N_d}(w)$ notwithstanding. This result shows that in terms of the warm layer, aerosols play a primary role in determining DSD characteristics.

The sensitivities to H are calculated in order to put the aerosol and updraft effects into perspective regarding cloud evolution. This calculation shows that, on average, droplet growth with cloud evolution is comparable in absolute value and is opposite to the aerosol effect. For this reason, studies

should take into account the altitude of the measurements. Polluted Amazonian clouds show slower droplet growth with altitude (Cecchini et al., 2016) and $S_{D_{\mathrm{eff}}}(H)$ values may vary with N_{a}. With lower $S_{D_{\mathrm{eff}}}(H)$, $S_{D_{\mathrm{eff}}}(N_{\mathrm{a}})$ values possibly increase with altitude. The most important factor evident in Table 3 for D_{eff} is that it shows strong relations with N_{a} and H, while being independent of w. This result is of great value for parameterizations or other analyses of cloud droplet size.

Whereas D_{eff} shows a clear relation to N_{a} and H, being relatively constant at fixed altitude, N_{d} displays a highly variable behavior. The averaged $S_{N_{\mathrm{d}}}(H)$ has a slightly negative value with high standard deviation. There can be either droplet depletion or production with altitude, but the former prevails on average. New droplet activation should be expected in polluted clouds, where not all aerosols are activated at cloud base. In fact, Table S6 shows that $S_{N_{\mathrm{d}}}(H)$ is positive for most polluted clouds probed when updraft speeds are $>0.5\,\mathrm{m\,s^{-1}}$, although R^2 values are quite low. Droplet depletion with altitude can be a result of evaporation and/or collection growth. Cecchini et al. (2016) showed that Amazonian background clouds present rather effective collision–coalescence growth, which would suggest a negative $S_{N_{\mathrm{d}}}(H)$ for those clouds. This mechanism is difficult to observe in the present study, with relatively low R^2 in the individual $S_{N_{\mathrm{d}}}(H)$ (Table S6). Overall, the highly variable relation between N_{d} and H suggests that droplet concentration is not closely tied to altitude above cloud base, as it is the case for D_{eff}. Conversely, droplet concentration has significant horizontal variation given different mixture and w conditions, while the effective diameter remains similar at constant altitude levels.

3.3 Effects on DSD shape and relation between sensitivities

The use of a parametric function to represent the DSDs can be of interest in order to understand the sensitivities in the overall shape of the DSDs. One function widely adopted in many applications and especially in models (Khain et al., 2015) is the gamma function. One of the forms of the gamma function represents the DSDs as

$$N(D) = N_0 D^{\mu} \exp(-\Lambda D), \tag{3}$$

in which N_0, μ, and Λ are intercept, shape, and curvature parameters, respectively. The advantage of using this function is that it can be analytically integrated, providing relatively simple equations for the DSD parameters. N_{d}, D_{eff}, and LWC can be calculated from the moments of the gamma DSD (units are $\mathrm{cm^{-3}}$, μm, and $\mathrm{g\,m^{-3}}$, respectively):

$$N_{\mathrm{d}} = M_0 \tag{4}$$

$$D_{\mathrm{eff}} = \frac{M_3}{M_2} \tag{5}$$

$$\mathrm{LWC} = 10^{-9}\rho_{\mathrm{w}}\frac{\pi}{6}M_3, \tag{6}$$

in which ρ_{w} is the density of liquid water (considered as $1000\,\mathrm{kg\,m^{-3}}$ here) and M_p is the pth moment of the DSD, given by

$$M_p = \int_0^{\infty} D^p N(D)\,\mathrm{d}D = N_0 \frac{\Gamma(\mu+p+1)}{\Lambda^{\mu+p+1}}. \tag{7}$$

By substituting Eq. (7) into (5) it is possible to write D_{eff} as a function of N_{d} and LWC:

$$D_{\mathrm{eff}} = 10^9 \frac{6}{\pi\rho_{\mathrm{w}}}\gamma\frac{\mathrm{LWC}}{N_{\mathrm{d}}}, \tag{8}$$

in which γ is a parameter that depends on the DSD shape and droplet size. It can be written as a function of ε, defined as the ratio between the DSD standard deviation and its average, which is much more common in the literature (e.g., Liu and Daum, 2002; Tas et al., 2015):

$$\gamma = \frac{\Lambda^2}{(\mu+2)(\mu+1)} = \frac{\Lambda\varepsilon^2}{D_a}. \tag{9}$$

D_a is the mean diameter resulting from the ratio between the second- and first-order moments. By substituting Eq. (9) into (8), applying the natural logarithm and the partial derivative to $\ln X_i$ (as in Eq. 1), it is possible to write

$$\frac{\partial \ln N_{\mathrm{d}}}{\partial \ln X_i} = \frac{\partial \ln \Lambda}{\partial \ln X_i} + 2\frac{\partial \ln \varepsilon}{\partial \ln X_i} + \frac{\partial \ln \mathrm{LWC}}{\partial \ln X_i} - 2\frac{\partial \ln D_{\mathrm{eff}}}{\partial \ln X_i}, \tag{10}$$

which is an explicit representation of the relation between the sensitivities. Note that $\frac{\partial \ln D_{\mathrm{eff}}}{\partial \ln X_i} = \frac{\partial \ln D_a}{\partial \ln X_i}$ because of the similarities in the equations of both diameters. The first two terms on the right-hand side in Eq. (10) represent the DSD shape, in which Λ is related to the curvature of the gamma curve and ε is the relative dispersion around the DSD mean geometric diameter. Lower (higher) Λ and higher (lower) ε values are associated with broader (narrower) DSDs. Equation (10) shows that, in order to compare the sensitivities in N_{d}, D_{eff}, and LWC, the DSD shape has to be taken into account.

Several aspects of the aerosol–cloud–interaction physics can be illustrated by Eq. (10). The Twomey effect states that clouds subject to high aerosol concentrations have enhanced albedo because of the more numerous droplets with increasing aerosol loading (Twomey, 1974). This effect is defined when comparing clouds with the same LWC. Translating it into Eq. (10) (with $X_i = N_{\mathrm{a}}$), it means that the LWC derivative is neglected, which defines a relation between droplet concentration, effective diameter, and DSD shape. By comparing to the expression $\overline{S_{D_{\mathrm{eff}}}(N_{\mathrm{a}})} = -\frac{1}{3}\overline{S_{N_{\mathrm{d}}}(N_{\mathrm{a}})}$ often found

Table 4. Same as Table 3, but for the sensitivities in Λ, ε, and LWC.

	$\overline{S_\Lambda}$	$\overline{S_\varepsilon}$	$\overline{S_{\mathrm{LWC}}}$
N_a	0.23 ± 0.34 $R^2 = 0.64$	-0.015 ± 0.16 $R^2 = 0.54$	0.078 ± 0.34 $R^2 = 0.34$
w	0.046 ± 0.17 $R^2 = 0.49$	0.039 ± 0.094 $R^2 = 0.46$	0.49 ± 0.34 $R^2 = 0.77$
H	-0.43 ± 0.32 $R^2 = 0.64$	0.094 ± 0.16 $R^2 = 0.42$	0.67 ± 0.21 $R^2 = 0.76$

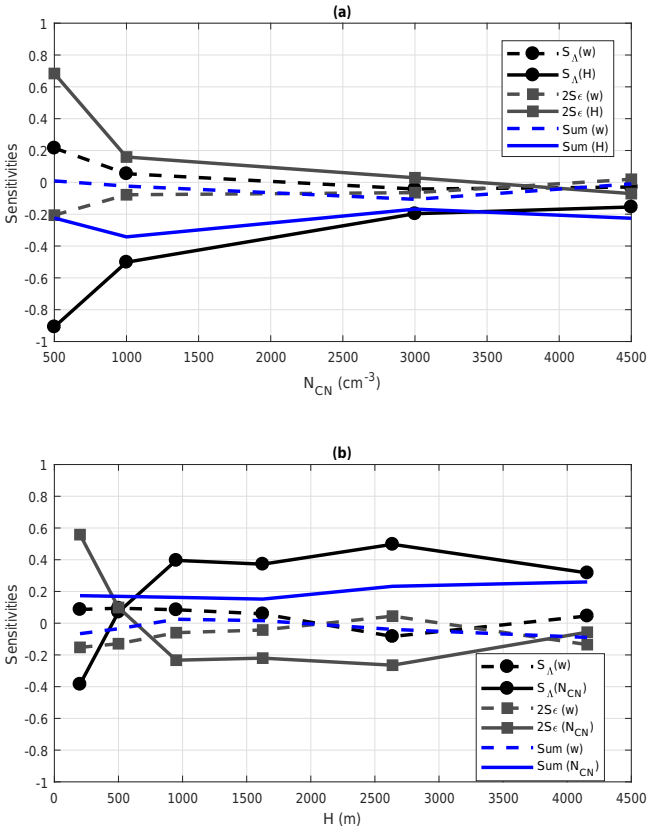

Figure 3. Variations in the sensitivities of Λ and ε with **(a)** N_a and **(b)** H. Note that the sensitivities of ε are multiplied by 2 in order to be consistent with Eq. (10). The curves are averaged over all values of the third dependent variable. For instance, the curve $S_\Lambda(w)$ in **(a)** is averaged over all H values. Blue curves represent the sum of the sensitivities of Λ and ε, equivalent to the first two terms on the right-hand side in Eq. (10).

in the literature, we can conclude that the value of the sensitivity of N_d to N_a is offset by some effect on DSD shape. In other words, two-thirds of the N_d sensitivity is allocated into DSD narrowing or broadening, while the remainder effectively alters D_eff.

The effects of enhanced aerosol concentrations on the DSD shape are of great interest to the climate change community, given that they contribute to the aerosol indirect effect. Liu and Daum (2002) report that pollution, in addition to lowering droplet size, tends to broaden the DSDs, which would result in weaker cooling forcing compared to previous calculations. They show that the previous estimations of the aerosol indirect effect considered a fixed ε, possibly overestimating the cooling forcing. Recently, Xie et al. (2017) reports improved model comparisons with satellites when better estimating the relative dispersion. Therefore, it is important to understand the relation between ε (and Λ) and not only aerosols but also updraft speed and height above cloud base. The overall averages presented in Table 4 show that the DSD curvature (Λ) is sensitive to N_a and H, but the values are rather small for ε. This results from the not-so-simple relation between DSD shape and N_a, w, and H. Figure 3 shows the variations in the sensitivities of Λ and ε with N_a and H (no significant variations were found for w), in which it is clear that the overall averages in Table 4 must be analyzed with caution for DSD shape. The ε sensitivities have a significantly different behavior for clean and polluted clouds and also change sign along H. Both features result in a low overall average as presented in Table 4, but this does not mean that the ε sensitivity is negligible. Instead, a more detailed analysis should be considered.

The sensitivities in Λ and ε usually have opposite signs, given their relation to DSD shape – broader DSDs tend to have higher ε values but lower Λ values. Nevertheless, their sensitivities to N_a and H are conceptually similar and illustrates interesting processes. Figure 3a shows that the DSD shape variation with altitude is much more pronounced in cleaner clouds, which is a result of a strong collision–coalescence process. The higher the aerosol concentration, the lower the sensitivity of ε to H. For the most polluted clouds measured by HALO, the relative dispersion parameter is almost insensitive to H, meaning that it does not change much as the cloud grows. There is, however, still some effect on the DSD curvature, making the summation of the first two terms on the right-hand side in Eq. (10) nonnegative in this case (see solid blue line in Fig. 3a). For the sensitivities of Λ and ε to w, the same summation (dashed line in Fig. 3a) is basically null, meaning that these two terms have no contribution in Eq. (10). Nevertheless, stronger updrafts tend to produce narrower DSDs in the maritime clouds in which the aerosol population is limited in terms of number concentration and particle type–chemistry.

The patterns along H of the DSD shape sensitivities (Fig. 3b) pose an interesting question for the parameterization of the aerosol indirect effect in Amazonian clouds. There are significant changes in ε tendencies as the clouds evolve. Note that aerosols induce broader DSDs up to $H \sim 500$ m, but the opposite happens above that point. In fact, for our higher-altitude bin ($2637\,\mathrm{m} < H \leq 4156\,\mathrm{m}$), the average ε is lowest for the most polluted clouds ($= 0.28$, while clouds over the forest and Atlantic Ocean show values of 0.32 and

0.42, respectively). In other words, the effect of broader DSDs under polluted conditions may not directly apply for convective clouds over the Amazon, where growth processes in the cloud can significantly change this pattern. This highlights the need to take cloud evolution into account and there is no direct relation between aerosols and cloud relative dispersion in the warm phase of Amazonian clouds. For satellite retrievals, in which integrated quantities are of likely interest, the relative dispersion will depend not only on the aerosol concentration but also on cloud depth and life cycle stage.

Regarding the sensitivities to w, Fig. 3 and Tables 3 and 4 show that updraft speed has little impact on DSD shape or droplet size. The result in terms of Eq. (10) is the equality between the sensitivities in N_d and LWC, which is generally the case when we compare the averages shown in Tables 3 and 4. In other words, the updraft effect is limited to increases in the droplet concentration and water content, modulating both N_d and LWC in the same proportion. Overall, the observations shown here should help understand which cloud properties are affected by aerosols, cloud evolution, and thermodynamic conditions. The latter was found to be associated with bulk water contents in the clouds, while the overall shape of the DSDs is determined by the aerosol condition during cloud formation and the subsequent evolution.

4 Concluding remarks

The ACRIDICON-CHUVA campaign and the capabilities of the HALO aircraft allowed the analysis of the sensitivities of Amazon tropical convective clouds to aerosol number concentrations and updraft speed while also considering cloud evolution. The sensitivity formulation identified that aerosol number concentrations play a primary role in the formation of the warm phase of convective clouds, determining not only droplet concentration but also diameter and overall DSD shape. Conversely, the thermodynamic conditions, as represented by the updraft intensity, affect primarily DSD bulk properties such as water content and droplet concentration. We have shown that the altitude above cloud base is critical when analyzing aerosol and updraft impacts on clouds, given that the DSD properties evolve with further processing in the system.

We showed that an increase of 100 % in aerosol concentration results in an 84 % increase in droplet number concentration on average, while the same relative increase in updraft wind speed results in only 43 % change. Regarding mean droplet size, we found it to be effectively independent of the updraft speed. Roughly, the effective droplet diameter decreases 25 % when aerosol concentration doubles. The comparison between the aerosol and the thermodynamic effects shows that the aerosol concentration is the primary driver for DSD, whereas the updrafts mainly affect droplet number concentration and liquid water content. During cloud evolution, droplet number concentration is depleted while the diameter sensitivity to the growth processes is quantitatively similar to the aerosol effect. Additionally, the aerosol effect on DSD shape inverts in sign with altitude, favoring broader droplet distributions close to cloud base but narrower droplet distributions higher in the clouds. This highlights the importance of differentiating the analysis by altitude above cloud base, which is an appropriate proxy for DSD lifetime for our measurements.

The results presented here can potentially be used to validate and derive new parameterizations in numerical models, which usually fail to correctly represent Amazonian convective clouds. One common issue of the models is the representation of the precipitation daily cycle, in which the modeled rainfall tends to occur earlier than in the observations. One possible reason for that is the misrepresentation of the cloud DSDs that can lead to artificially high efficiency in rain formation. Therefore, model runs can be performed in order to assess the factors that control DSD formation, and comparisons can be made with our results as a benchmark. The analysis of the ε and Λ parameters can be especially useful in that regard. The results presented here detail several aspects of the Amazonian clouds and their relation to aerosol and thermodynamic conditions. For instance, it was shown that aerosols can induce DSD broadening only close to cloud base, preferably under high w conditions. Higher in the clouds, increased aerosol loading leads to DSD narrowing. Additionally, DSD broadening with altitude is pronounced only in clean clouds, in which the collection processes are efficient. The result is growing ε with altitude, while this parameter remains relatively constant with H in polluted clouds. Good models should be able to reproduce such details in order to generate better forecasts. Therefore, we believe the results presented here can be of use for that purpose, by providing specificities of Amazonian clouds that models should aim to reproduce.

Data availability. The data used in this study can be found at https://halo-db.pa.op.dlr.de/mission/5.

The Supplement related to this article is available online at https://doi.org/10.5194/acp-17-10037-2017-supplement.

Competing interests. The authors declare that they have no conflict of interest.

Special issue statement. This article is part of the special issue "The ACRIDICON-CHUVA campaign to study deep convective clouds and precipitation over Amazonia using the new German HALO research aircraft (ACP/AMT inter-journal SI)". It is not associated with a conference.

This article is part of the special issue "BACCHUS – Impact

of Biogenic versus Anthropogenic emissions on Clouds and Climate: towards a Holistic UnderStanding (ACP/AMT/GMD inter-journal SI)". It is not associated with a conference.

This article is part of the special issue "Observations and Modeling of the Green Ocean Amazon (GoAmazon2014/5) (ACP/AMT/GI/GMD inter-journal SI)". It is not associated with a conference.

Acknowledgements. The ACRIDICON-CHUVA campaign was supported by the Max Planck Society (MPG), the German Science Foundation (DFG Priority Program SPP 1294), the German Aerospace Center (DLR), the FAPESP (Sao Paulo Research Foundation) (grants 2009/15235-8 and 2013/05014-0), and a wide range of other institutional partners. It was carried out in collaboration with the USA–Brazilian atmosphere research project GoAmazon2014/5, including numerous institutional partners. We would like to thank the Instituto Nacional de Pesquisas da Amazonia (INPA) for local logistic help prior, during, and after the campaign. Thanks also to the Brazilian Space Agency (AEB: Agencia Espacial Brasileira), who were responsible for the program of cooperation (CNPq license 00254/2013–9 of the Brazilian National Council for Scientific and Technological Development). The contribution of Daniel Rosenfeld was supported by project BACCHUS European Commission FP7-603445. Micael A. Cecchini was funded by FAPESP grants 2014/08615-7 and 2014/21189-7. B. Weinzierl would like to acknowledge funding from the Helmholtz Association (grant no. VH-NG-606, AerCARE) and from the European Research Council under the European Community's Horizon 2020 research and innovation framework program/ERC grant agreement 640458 (A-LIFE). The entire ACRIDICON-CHUVA project team is gratefully acknowledged for collaboration and support. The data used in this study can be found at http://www.halo.dlr.de/halo-db/. We would also like to acknowledge the contributions from the two anonymous referees that greatly improved the quality of this paper.

Edited by: Stuart A. Penkett
Reviewed by: two anonymous referees

References

Andreae, M. O., Rosenfeld, D., Artaxo, P., Costa, A. A., Frank, G. P., Longo, K. M., and Silva-Dias, M. A. F.: Smoking Rain Clouds over the Amazon, Science, 303, 1337–1342, 2004.

Artaxo, P., Martins, J. V., Yamasoe, M. A., Procópio, A. S., Pauliquevis, T. M., Andreae, M. O., Guyon, P., Gatti, L. V., and Leal, A. M. C.: Physical and chemical properties of aerosols in the wet and dry seasons in Rondônia, Amazonia, J. Geophys. Res., 107, 8081, https://doi.org/10.1029/2001JD000666, 2002.

Berg, L. K., Berkowitz, C. M., Barnard, J. C., Senum, G., and Springston, S. R.: Observations of the first aerosol indirect effect in shallow cumuli, Geophys. Res. Lett., 38, L03809, https://doi.org/10.1029/2010GL046047, 2011.

Bréon, F., Tanré, D., and Generoso, S.: Aerosol effect on cloud droplet size monitored from satellite, Science, 295, 834–838, https://doi.org/10.1126/science.1066434, 2002.

Bulgin, C. E., Palmer, P. I., Thomas, G. E., Arnold, C. P. G., Campmany, E., Carboni, E., Grainger, R. G., Poulsen, C., Siddans, R., and Lawrence, B. N.: Regional and seasonal variations of the Twomey indirect effect as observed by the ATSR-2 satellite instrument, Geophys. Res. Lett., 35, L02811, https://doi.org/10.1029/2007GL031394, 2008.

Cecchini, M. A., Machado, L. A. T., Comstock, J. M., Mei, F., Wang, J., Fan, J., Tomlinson, J. M., Schmid, B., Albrecht, R., Martin, S. T., and Artaxo, P.: Impacts of the Manaus pollution plume on the microphysical properties of Amazonian warm-phase clouds in the wet season, Atmos. Chem. Phys., 16, 7029–7041, https://doi.org/10.5194/acp-16-7029-2016, 2016.

Chang, D., Cheng, Y., Reutter, P., Trentmann, J., Burrows, S. M., Spichtinger, P., Nordmann, S., Andreae, M. O., Pöschl, U., and Su, H.: Comprehensive mapping and characteristic regimes of aerosol effects on the formation and evolution of pyro-convective clouds, Atmos. Chem. Phys., 15, 10325–10348, https://doi.org/10.5194/acp-15-10325-2015, 2015.

Fan, J., Yuan, T., Comstock, J. M., Ghan, S., Khain, A., Leung, L. R., Li, Z., Martins, V. J., and Ovchinnikov, M.: Dominant role by vertical wind shear in regulating aerosol effects on deep convective clouds, J. Geophys. Res.-Atmos., 114, D22206, https://doi.org/10.1029/2009JD012352, 2009.

Feingold, G.: Modeling of the first indirect effect: Analysis of measurement requirements, Geophys. Res. Lett., 30, 1997, https://doi.org/10.1029/2003GL017967, 2003.

Fisch, G., Tota, J., Machado, L. A. T., Dias, M., Lyra, R. F. D., Nobre, C. A., Dolman, A. J., and Gash, J. H. C.: The convective boundary layer over pasture and forest in Amazonia, Theor. Appl. Climatol., 78, 47–59, 2004.

Freud, E. and Rosenfeld, D.: Linear relation between convective cloud drop number concentration and depth for rain initiation, J. Geophys. Res., 117, D02207, https://doi.org/10.1029/2011JD016457, 2012.

Freud, E., Rosenfeld, D., and Kulkarni, J. R.: Resolving both entrainment-mixing and number of activated CCN in deep convective clouds, Atmos. Chem. Phys., 11, 12887-12900, doi:10.5194/acp-11-12887-2011, 2011.

Hallquist, M., Wenger, J. C., Baltensperger, U., Rudich, Y., Simpson, D., Claeys, M., Dommen, J., Donahue, N. M., George, C., Goldstein, A. H., Hamilton, J. F., Herrmann, H., Hoffmann, T., Iinuma, Y., Jang, M., Jenkin, M. E., Jimenez, J. L., Kiendler-Scharr, A., Maenhaut, W., McFiggans, G., Mentel, Th. F., Monod, A., Prévôt, A. S. H., Seinfeld, J. H., Surratt, J. D., Szmigielski, R., and Wildt, J.: The formation, properties and impact of secondary organic aerosol: current and emerging issues, Atmos. Chem. Phys., 9, 5155–5236, https://doi.org/10.5194/acp-9-5155-2009, 2009.

Heymsfield, A. J., Bansemer, A., Heymsfield, G., and Fierro, A. O.: Microphysics of maritime tropical convective updrafts at temperatures from -20° C to -60° C, J. Atmos. Sci., 66, 3530–3562, https://doi.org/10.1175/2009JAS3107.1, 2009.

Kanakidou, M., Tsigaridis, K., Dentener, F. J., and Crutzen, P. J.: Human-activity-enhanced formation of organic aerosols by biogenic hydrocarbon oxidation, J. Geophys. Res.-Atmos., 105, 9243–9254, 2000.

Karydis, V. A., Capps, S. L., Russell, A. G., and Nenes, A.: Adjoint sensitivity of global cloud droplet number to aerosol and

dynamical parameters, Atmos. Chem. Phys., 12, 9041–9055, https://doi.org/10.5194/acp-12-9041-2012, 2012.

Kay, J. E. and Wood, R.: Timescale analysis of aerosol sensitivity during homogeneous freezing and implications for upper tropospheric water vapor budgets, Geophys. Res. Lett., 35, L10809, https://doi.org/10.1029/2007gl032628, 2008.

Khain, A. P., Beheng, K. D., Heymsfield, A., Korolev, A., Krichak, S. O., Levin, Z., Pinsky, M., Phillips, V., Prabhakaran, T., Teller, A., van den Heever, S. C., and Yano, J.-I.: Representation of microphysical processes in cloud-resolving models: spectral (bin) microphysics versus bulk parameterization, Rev. Geophys. 53, 247–322, https://doi.org/10.1002/2014RG000468, 2015.

Kidd, C., Dawkins, E., and Huffman, G.: Comparison of precipitation derived from the ECMWF operational forecast model and satellite precipitation datasets, J. Hydrometeor., 14, 1463–1482, https://doi.org/10.1175/JHM-D-12-0182.1, 2013.

Klingebiel, M., de Lozar, A., Molleker, S., Weigel, R., Roth, A., Schmidt, L., Meyer, J., Ehrlich, A., Neuber, R., Wendisch, M., and Borrmann, S.: Arctic low-level boundary layer clouds: in situ measurements and simulations of mono- and bimodal supercooled droplet size distributions at the top layer of liquid phase clouds, Atmos. Chem. Phys., 15, 617–631, https://doi.org/10.5194/acp-15-617-2015, 2015.

Korolev, A.: Reconstruction of the Sizes of Spherical Particles from Their Shadow Images. Part I: Theoretical Considerations, J. Atmos. Ocean. Tech., 24, 376–389, https://doi.org/10.1175/JTECH1980.1, 2007, 2007.

Korolev, A., Khain, A., Pinsky, M., and French, J.: Theoretical study of mixing in liquid clouds – Part 1: Classical concepts, Atmos. Chem. Phys., 16, 9235–9254, https://doi.org/10.5194/acp-16-9235-2016, 2016.

Kuhn, U., Ganzeveld, L., Thielmann, A., Dindorf, T., Schebeske, G., Welling, M., Sciare, J., Roberts, G., Meixner, F. X., Kesselmeier, J., Lelieveld, J., Kolle, O., Ciccioli, P., Lloyd, J., Trentmann, J., Artaxo, P., and Andreae, M. O.: Impact of Manaus City on the Amazon Green Ocean atmosphere: ozone production, precursor sensitivity and aerosol load, Atmos. Chem. Phys., 10, 9251–9282, https://doi.org/10.5194/acp-10-9251-2010, 2010.

Lance, S., Brock, C. A., Rogers, D., and Gordon, J. A.: Water droplet calibration of the Cloud Droplet Probe (CDP) and in-flight performance in liquid, ice and mixed-phase clouds during ARCPAC, Atmos. Meas. Tech., 3, 1683–1706, https://doi.org/10.5194/amt-3-1683-2010, 2010.

Liu, Y. and Daum, P. H.: Anthropogenic aerosols: Indirect warming effect from dispersion forcing, Nature, 419, 580–581, https://doi.org/10.1038/419580a, 2002.

Machado, L. A. T., Silva Dias, M. A. F., Morales, C., Fisch, G., Vila, D., Albrecht, R. I., Goodman, S. J., Calheiros, A. J. P., Biscaro, T., Kummerow, C., Cohen, J., Fitzjarrald, D., Nascimento, E. L., Sakamoto, M. S., Cunningham, C., Chaboureau, J.-P., Petersen, W. A., Adams, D. K., Baldini, L., Angelis, C. F., Sapucci, L. F., Salio, P., Barbosa, H. M. J., Landulfo, E., Souza, R. A. F., Blakeslee, R. J., Bailey, J., Freitas, S., Lima, W. F. A., and Tokay, A.: The Chuva Project: How Does Convection Vary across Brazil?, B. Amer. Meteorol. Soc., 95, 1365–1380, 2014.

Mallaun, C., Giez, A., and Baumann, R.: Calibration of 3-D wind measurements on a single-engine research aircraft, Atmos. Meas. Tech., 8, 3177–3196, https://doi.org/10.5194/amt-8-3177-2015, 2015.

Martin, G. M., Johnson, D. W., and Spice, A.: The measurement and parameterization of effective radius of droplets in warm stratocumulus clouds, J. Atmos. Sci., 51, 1823–1842, https://doi.org/10.1029/2011JD016532, 1994.

Martin, S. T., Andreae, M. O., Artaxo, P., Baumgardner, D., Chen, Q., Goldstein, A. H., Guenther, A., Heald, C. L., Mayol-Bracero, O. L., McMurry, P. H., Pauliquevis, T., Pöschl, U., Prather, K. A., Roberts, G. C., Saleska, S. R., Silva Dias, M. A., Spracklen, D. V., Swietlicki, E., and Trebs, I.: Sources and properties of Amazonian aerosol particles, Rev. Geophys., 48, RG2002, https://doi.org/10.1029/2008RG000280, 2010.

Martin, S. T., Artaxo, P., Machado, L. A. T., Manzi, A. O., Souza, R. A. F., Schumacher, C., Wang, J., Andreae, M. O., Barbosa, H. M. J., Fan, J., Fisch, G., Goldstein, A. H., Guenther, A., Jimenez, J. L., Pöschl, U., Silva Dias, M. A., Smith, J. N., and Wendisch, M.: Introduction: Observations and Modeling of the Green Ocean Amazon (GoAmazon2014/5), Atmos. Chem. Phys., 16, 4785–4797, https://doi.org/10.5194/acp-16-4785-2016, 2016.

McFiggans, G., Artaxo, P., Baltensperger, U., Coe, H., Facchini, M. C., Feingold, G., Fuzzi, S., Gysel, M., Laaksonen, A., Lohmann, U., Mentel, T. F., Murphy, D. M., O'Dowd, C. D., Snider, J. R., and Weingartner, E.: The effect of physical and chemical aerosol properties on warm cloud droplet activation, Atmos. Chem. Phys., 6, 2593–2649, https://doi.org/10.5194/acp-6-2593-2006, 2006.

Molleker, S., Borrmann, S., Schlager, H., Luo, B., Frey, W., Klingebiel, M., Weigel, R., Ebert, M., Mitev, V., Matthey, R., Woiwode, W., Oelhaf, H., Dörnbrack, A., Stratmann, G., Grooß, J.-U., Günther, G., Vogel, B., Müller, R., Krämer, M., Meyer, J., and Cairo, F.: Microphysical properties of synoptic-scale polar stratospheric clouds: in situ measurements of unexpectedly large HNO_3-containing particles in the Arctic vortex, Atmos. Chem. Phys., 14, 10785–10801, https://doi.org/10.5194/acp-14-10785-2014, 2014.

Pandithurai, G., Dipu, S., Prabha, T. V., Maheskumar, R. S., Kulkarni, J. R., and Goswami, B. N.: Aerosol effect on droplet spectral dispersion in warm continental cumuli, J. Geophys. Res., 117, D16202, https://doi.org/10.1029/2011JD016532, 2012.

Pöschl, U., Martin, S. T., Sinha, B., Chen, Q., Gunthe, S. S., Huffman, J. A., Borrmann, S., Farmer, D. K., Garland, R. M., Helas, G., Jimenez, J. L., King, S. M., Manzi, A., Mikhailov, E., Pauliquevis, T., Petters, M. D., Prenni, A. J., Roldin, P., Rose, D., Schneider, J., Su, H., Zorn, S. R., Artaxo, P., and Andreae, M. O.: Rainforest aerosols as biogenic nuclei of clouds and precipitation in the Amazon, Science, 329, 1513–1516, doi:10.1126/science.1191056, 2010.

Quaas, J., Boucher, O., and Breon, F.: Aerosol indirect effects in POLDER satellite data and the Laboratoire de Meteorologie Dynamique-Zoom (LMDZ) general circulation model, J. Geophys. Res., 109, D08205, https://doi.org/10.1029/2003JD004317, 2004.

Reutter, P., Su, H., Trentmann, J., Simmel, M., Rose, D., Gunthe, S. S., Wernli, H., Andreae, M. O., and Pöschl, U.: Aerosol- and updraft-limited regimes of cloud droplet formation: influence of particle number, size and hygroscopicity on the activation of cloud condensation nuclei (CCN), Atmos. Chem. Phys., 9, 7067–7080, https://doi.org/10.5194/acp-9-7067-2009, 2009.

Roberts, G. C. and Nenes, A.: A Continuous-Flow Streamwise Thermal-Gradient CCN Chamber for Atmospheric

Measurements, Aerosol Sci. Technol., 39, 206–221, https://doi.org/10.1080/027868290913988, 2005.

Rose, D., Gunthe, S. S., Mikhailov, E., Frank, G. P., Dusek, U., Andreae, M. O., and Pöschl, U.: Calibration and measurement uncertainties of a continuous-flow cloud condensation nuclei counter (DMT-CCNC): CCN activation of ammonium sulfate and sodium chloride aerosol particles in theory and experiment, Atmos. Chem. Phys., 8, 1153–1179, https://doi.org/10.5194/acp-8-1153-2008, 2008.

Rosenfeld, D., Zheng, Y., Hashimshoni, E., Pöhlker, M. L., Jefferson, A., Pöhlker, C., Yu, X., Zhu, Y., Liu, G., Yue, Z., Fischman, B., Li, Z., Giguzin, D., Goren, T., Artaxo, P., Barbosa, H. M. J., Pöschl, U., and Andreae, M. O.: Satellite retrieval of cloud condensation nuclei concentrations by using clouds as CCN chambers, P. Natl. Acad. Sci. USA, 113, 5828–5834, 2016.

Schmidt, J., Ansmann, A., Bühl, J., and Wandinger, U.: Strong aerosol-cloud interaction in altocumulus during updraft periods: lidar observations over central Europe, Atmos. Chem. Phys., 15, 10687–10700, https://doi.org/10.5194/acp-15-10687-2015, 2015.

Seinfeld, J. H., Bretherton, C., Carslaw, K. S., Coe, H., DeMott, P. J., Dunlea, E. J., Feingold, G., Ghan, S., Guenther, A. B., Kahn, R., Kraucunas, I., Kreidenweis, S. M., Molina, M. J., Nenes, A., Penner, J. E., Prather, K. A., Ramanathan, V., Ramaswamy, V., Rasch, P. J., Ravishankara, A. R., Rosenfeld, D., Stephens, G., and Wood, R.: Improving our fundamental understanding of the role of aerosol-cloud interactions in the climate system, P. Natl. Acad. Sci. USA, 113, 5781–5790, 2016.

Sorooshian, A., Feingold, G., Lebsock, M. D., Jiang, H. L., and Stephens, G. L.: On the precipitation susceptibility of clouds to aerosol perturbations, Geophys. Res. Lett., 36, L13803, https://doi.org/10.1029/2009gl038993, 2009.

Sullivan, S. C., Lee, D., Oreopoulos, L., and Nenes, A.: Role of updraft velocity in temporal variability of global cloud hydrometeor number, P. Natl. Acad. Sci. USA, 113, 5791–5796, 2016.

Tas, E., Teller, A., Altaratz, O., Axisa, D., Bruintjes, R., Levin, Z., and Koren, I.: The relative dispersion of cloud droplets: its robustness with respect to key cloud properties, Atmos. Chem. Phys., 15, 2009–2017, https://doi.org/10.5194/acp-15-2009-2015, 2015.

Twomey, S.: The nuclei of natural cloud formation part II: The supersaturation in natural clouds and the variation of cloud droplet concentration, Geofis. Pura Appl., 43, 243–249, 1959.

Twomey, S.: Pollution and the planetary albedo, Atmos. Environ., 8, 1251–1256, https://doi.org/10.1016/0004-6981(74)90004-3, 1974.

Vogelmann, A., McFarquhar, G., Ogren, J., Turner, D., Comstock, J., Feingold, G., Long, C., Jonsson, H., Bucholtz, A., Collins, D., Diskin, G., Gerber, H., Lawson, R., Woods, R., Andrews, E., Yang, H., Chiu, J., Hartsock, D., Hubbe, J., Lo, C., Marshak, A., Monroe, J., McFarlane, S., Schmid, B., Tomlinson, J., and Toto, T.: Racoro Extended-Term Aircraft Observations of Boundary Layer Clouds, B. Am. Meteorol. Soc., 93, 861–878, https://doi.org/10.1175/BAMS-D-11-00189.1, 2012.

Wang, J., Krejci, R., Giangrande, S., Kuang, C., Barbosa, H. M. J., Brito, J., Carbone, S., Chi, X., Comstock, J., Ditas, F., Lavric, J., Manninen, H. E., Mei, F., Moran-Zuloaga, D., Pöhlker, C., Pöhlker, M. L., Saturno, J., Schmid, B., Souza, R. A. F., Springston, S. R., Tomlinson, J. M., Toto, T., Walter, D., Wimmer, D., Smith, J. N., Kulmala, M., Machado, L. A. T., Artaxo, P., Andreae, M. O., Petäjä, T., and Martin, S. T.: Vertical transport during rainfall sustains aerosol concentration in Amazon boundary layer, Nature, 539, 416–419, https://doi.org/10.1038/nature19819, 2016.

Wendisch, M., Pöschl, U., Andreae, M. O., Machado, L. A. T., Albrecht, R., Schlager, H., Rosenfeld, D., Martin, S. T., Abdelmonem, A., Afchine, A., Araújo, A., Artaxo, P., Aufmhoff, H., Barbosa, H. M. J., Borrmann, S., Braga, R., Buchholz, B., Cecchini, M. A., Costa, A., Curtius, J., Dollner, M., Dorf, M., Dreiling, V., Ebert, V., Ehrlich, A., Ewald, F., Fisch, G., Fix, A., Frank, F., Fütterer, D., Heckl, C., Heidelberg, F., Hüneke, T., Jäkel, E., Järvinen, E., Jurkat, T., Kanter, S., Kästner, U., Kenntner, M., Kesselmeier, J., Klimach, T., Knecht, M., Kohl, R., Kölling, T., Krämer, M., Krüger, M., Krisna, T. C., Lavric, J. V., Longo, K., Mahnke, C., Manzi, A. O., Mayer, B., Mertes, S., Minikin, A., Molleker, S., Münch, S., Nillius, B., Pfeilsticker, K., Pöhlker, C., Roiger, A., Rose, D., Rosenow, D., Sauer, D., Schnaiter, M., Schneider, J., Schulz, C., de Souza, R. A. F., Spanu, A., Stock, P., Vila, D., Voigt, C., Walser, A., Walter, D., Weigel, R., Weinzierl, B., Werner, F., Yamasoe, M. A., Ziereis, H., Zinner, T., and Zöger, M.: The ACRIDICON-CHUVA campaign: Studying tropical deep convective clouds and precipitation over Amazonia using the new German research aircraft HALO, B. Am. Meteorol. Soc., 97, 1885–1908, https://doi.org/10.1175/BAMS-D-14-00255.1, 2016.

Werner, F., Ditas, F., Siebert, H., Simmel, M., Wehner, B., Pilewskie, P., Schmeissner, T., Shaw, R. A., Hartmann, S., Wex, H., Roberts, G. C., and Wendisch, M.: Twomey effect observed from collocated microphysical and remote sensing measurements over shallow cumulus, J. Geophys. Res., 119, 1534–1545, https://doi.org/10.1002/2013JD020131, 2014.

Xie, X., Zhang, H., Liu, X., Peng, Y., and Liu, Y.: Sensitivity study of cloud parameterizations with relative dispersion in CAM5.1: impacts on aerosol indirect effects, Atmos. Chem. Phys., 17, 5877–5892, https://doi.org/10.5194/acp-17-5877-2017, 2017.